

## Control and management of a fuel cell microgrid. Energy efficiency optimization

J.I. San Martín<sup>1</sup>, I. Zamora<sup>2</sup>, F.J. Asensio<sup>2</sup>, J. García-Villalobos<sup>2</sup>, J.J. San Martín<sup>1</sup> V. Aperribay<sup>1</sup>.

Department of Electrical Engineering - University of the Basque Country (UPV/EHU)

<sup>1</sup> Escuela de Ingeniería de Eibar  
 Avda. Otaola, 29, 20600 Eibar (Spain)  
 e\_mail: josegnacio.sanmartin@ehu.es

<sup>2</sup> Escuela Técnica Superior de Ingeniería de Bilbao  
 Alda. Urquijo s/n, 48013 Bilbao (Spain)  
 e\_mail: immaculada.zamora@ehu.es

**Abstract.** Increasing the efficiency of energy conversion systems is a relevant aspect to decrease the oil dependence and to minimize environmental impact. Considering the inherent characteristics of the PEM fuel cells, this paper proposes a control algorithm for a microgrid consisting of two fuel cells, in order to improve its energy efficiency. To do this, hardware responsible for managing the microgrid has been designed and implemented and the proposed control algorithm has been applied. Various tests have been performed on the microgrid, analysing its behaviour in each case.

### Key words

Control, Efficiency, Fuel Cells, Microgrid, PEMFC.

### 1. Introduction

According to the International Energy Agency (IEA), energy efficiency is the cheapest and the most appropriate way of tackling the challenges of the energy model, primarily to climate change mitigation. The main objective is to achieve a 450 ppm of CO<sub>2</sub> emission scenario, which limits the increase in global temperature below 2°C and poses a reduction of global greenhouse gas (GHG) emissions, by 2050, close to 50% compared to 1990. Energy efficiency is presented as the main tool, responsible for almost 60% of the emission reduction [1]. Thus, energy efficiency is seen as a key element to face up to climate change.

For this reason, European Union has developed the Energy Saving and Efficiency Action Plan 2011-2020, which complies with the requirements of Directive 2006/32/EC on energy services end-use efficiency. This Directive sets a minimum indicative energy savings aim around 9% in 2016 [2]. Moreover, EU has adopted the Action Plan for Energy Efficiency (2007-2012) aimed at reducing energy consumption around 20% by 2020. This objective corresponds to achieving savings around 1.5% per year, by 2020.

In this context, it is necessary to develop new techniques and products that are efficient in terms of energy, in order

to make significant energy savings. With this purpose, a control system which optimizes power delivery of a fuel cell based microgrid, and thus its efficiency, has been developed. Also, a boost converter has been designed and implemented.

Moreover, to accurately assess the energy performance and optimize integration and control strategies, experimental tests have been developed on a microgrid composed of two commercial PEM fuel cells: The Nexa Power Module [3] and Nexa Training System [4], of 1.2 kW<sub>e</sub> each one.

In this paper, both the developments made and the results obtained are presented.

### 2. Micro-grid design

#### A. General scheme

Figure 1 shows the complete diagram of the microgrid consisting of the two fuel cells indicated above. These fuel cells are supplied by two 50-liter hydrogen bottles, at 200 bar pressure. As additional power source, three metal hydride bottles of 6.4 kg of H<sub>2</sub> each, at 10 bar pressure, are available.

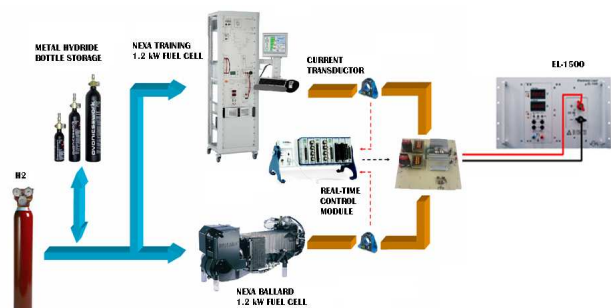


Fig. 1. General structure of the micro-grid system.

All the energy from the fuel cells is managed by two Boost type converters, which are controlled by a real-

time control module cRIO-9073 [5][6]. The real-time controller manages the duty cycle triggers of each converter, depending on the output voltage, the current delivered by each fuel cell and the operational temperature of each fuel cell.

As the microgrid load, two EL-1500 electronic loads have been used, of 1.5 kW each one. Both electronic loads are controlled by LabVIEW software, so the power demand can be adjusted at any time. This option has allowed developing the experiments to verify the correct operation of the microgrid, based on the power to be delivered.

### B. Boost converters

The regulated voltage generated by the Nexa System Training and the Nexa Power Module (input voltages to boost), when operating in no-load conditions, are 27.7 V and 26.3 V respectively. The boost converters used in the electrical microgrid increase and stabilize this voltage from the fuel cell. Thus, these voltages are increased to 30 V, so that they can feed a stabilized voltage to the voltage inverter. Moreover, these converters manage the energy generated by each fuel cell system.

The major advantage of this converter architecture is the ability to increase the output voltage related to the input one, by a factor up to 10, without the need of a transformer. The use of an inductor is normally more economical in comparison to a transformer. Assuming the DC bus voltage constant and that fuel cells operate delivering full power, the duty cycle of each converter is 0.156 and 0.141. The more restrictive of these two duty cycles is the highest one. Therefore, it is used when performing calculations for obtaining the coil inductance and the capacitor capacity. Following, the main components of the boost converter are presented.

#### 1) Inductor

When fuel cells operate at nominal power, they deliver 40 A. Anyway, from 1 A of consumption in the load, a continuous current through the coil is required. To avoid a large current ripple at the output, a minimum current is established considering that the ripple current does not exceed 1% of the current value.

Thus, the value of the inductance is obtained (equation (1)), taking into account a switching frequency of MOSFETs in the converter of 20 kHz and considering a continuous current.

$$L \geq \frac{V_i^2 \cdot D}{2 \cdot V_o \cdot I_{o_{\min}} \cdot f} = \frac{25,3^2 \cdot 0,156}{2 \cdot 30 \cdot 0,99 \cdot 20 \cdot 10^3} = 84,05 \mu H \quad (1)$$

From the numerical value obtained in (1), a coil of 100  $\mu H$  has been chosen, since it is the commercial device that best meets the requirements. This chosen coil is shown in [7].

#### 2) Capacitor

From the inductance value obtained, the capacitor value is calculated considering that the ripple in the boost output voltage is 3% of the DC bus voltage, as shown in equation (2).

$$\frac{\Delta V_o}{V_o} = \frac{\Delta Q}{C \cdot V_o} = \frac{I_o \cdot D \cdot T}{C \cdot V_o} = \frac{I_o \cdot D}{C \cdot V_o \cdot f} = \frac{40 \cdot 0,156}{C \cdot 30 \cdot 20 \cdot 10^3} \quad (2)$$

A 470  $\mu F$  capacitor has been chosen as it is the commercial solution that best fits the requirements. The chosen capacitor is shown in [8].

#### 3) Diode

The needed diode for this application must have a small reverse recovery, because the switching frequency at which it will operate is 20 kHz. Additionally, the current that has to be able to withstand is at least 40 A. With these performance requirements, a commercial solution is reached, choosing a Schottky power rectifier diode, shown in [9].

#### 4) MOSFET

For the MOSFET selection, the maximum current will have to be around 40 A. The MOSFET has to govern some of that current depending on the duty cycle. Also, the maximum voltage in the DC bus, will be 30 V when the diode is on. Given these characteristics, the MOSFET chosen is shown in [10].

Additionally, considering the switching frequency of 20 kHz, which correspond to a period approximately 170 times greater than the sum of all the MOSFET switching times, the system may be operated properly with different duty cycles.

Finally, as the gate voltage of the MOSFET is 15 V, and the signal available from the cRIO-9073 is 5V TTL format, the driver shown in [11] has been chosen to amplify that gate voltage. This way, it is possible to supply enough current for the proper switching.

### C. Simulation with PSIM

Before implementing the physical design of the boost converter, simulations have been performed with PSIM software to verify the correct operation of the converters in the microgrid's system (Figure 2). The fuel cells and the buck converter have been modeled as power sources that vary the voltage, depending on the power supplied to the load. Also, power delivered by each fuel cell has been limited up to 1066.5 W.

Different simulations have been performed to know the approximate response to changes in system load and the current reference of the current controlled boost.

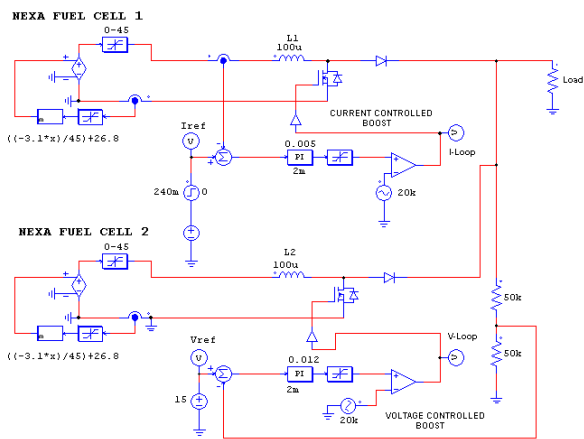


Fig. 2. Microgrid model in PSIM.

In the first case, the system starts without load (Figure 3). The capacitors are considered charged to 26.5 V, which is the voltage of the fuel cell batteries in the actual circuit. Simulation results show that the output voltage is stabilized quickly in 30 V, while the current control loop remains at 0 A as the reference.

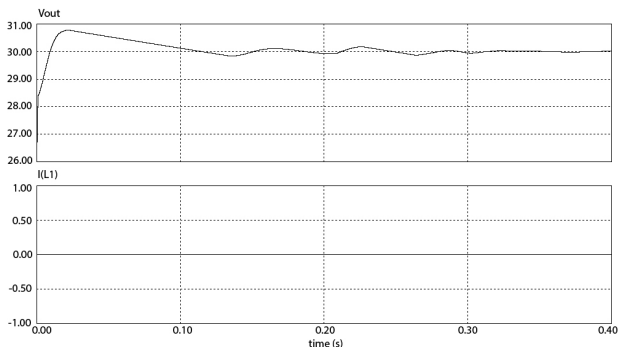


Fig. 3. Boost converters starting with no-load.

In the following test case a system starting with 225 W of load is simulated. As can be seen in Figure 4, the voltage has an output voltage ripple that drops gradually. The maximum ripple in steady state is slightly higher than 0.01 V. Two frequencies in the ripple can be observed, one of 20 kHz which corresponds to the switching of the MOSFETs and the other of approximately 550 Hz due to the control.

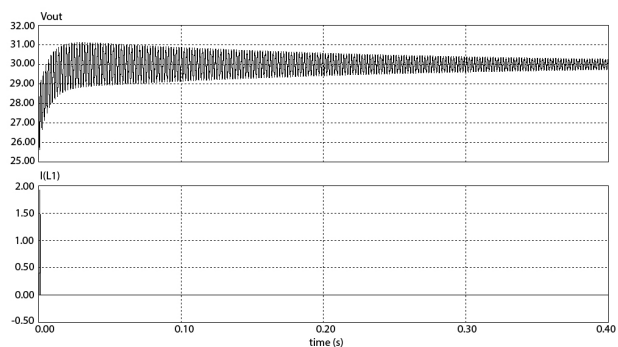


Fig. 4. Boost converters starting with load.

Figure 5 shows the results when a load of 600 W is connected at 220 ms. This demanded power is supplied by the boost operating in voltage mode. At  $t = 240$  ms, a

setpoint of 20 A is applied to the boost operating in current mode, so that the system is supplying 1200 W. It can be seen that the voltage drop only affects the converter that performs the voltage mode control.

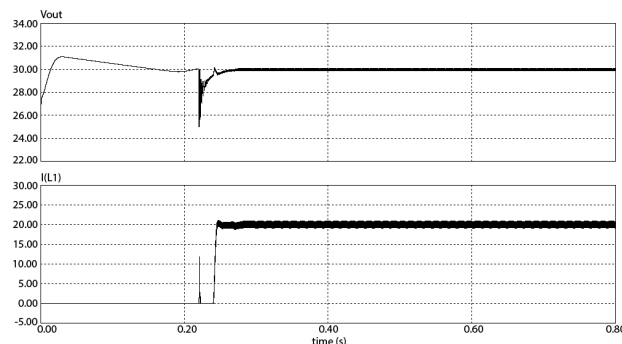


Fig. 5. Connection of a load of 600 W and set-point change to 20 A.

When an instantaneous power of 600 W is demanded, there is a voltage drop to 25V, which is stabilized to 30V in 20 ms. It can be seen how the control system responds properly to these set-point changes and demand, adapting to the new set-points within milliseconds.

### 3. Control and management

#### A. Control board design

Once the components have been calculated individually for each converter and the operation has been verified by simulation, the final disposition of the two converters is performed. This design includes the implementation of the converters, MOSFETs drivers, fuses, connection to the two fuel cell inputs and the output corresponding to the union of the two boost. To do the PCB layout, the system is built on ISIS and ARES Proteus software, which are design and simulation software tools for digital electronic systems. Figure 6 shows the physical implementation of the PCB with the components.

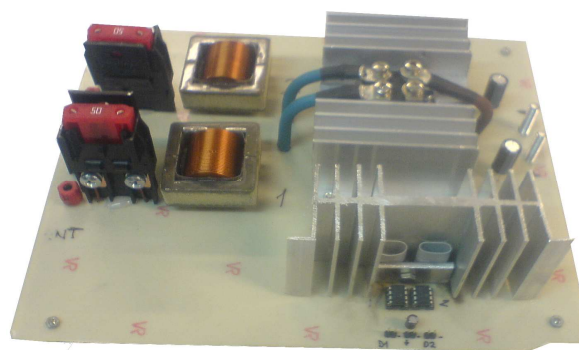


Fig. 6. Physical implementation of the boost converters.

#### B. Control strategy definition

Before defining the control strategy, experimental tests have been developed to know the optimal efficiency of the fuel cells in terms of power generated and operating temperature. Figure 7 shows the efficiency curve of the PEM fuel cells considered, which is optimal when they deliver 30% of the nominal power (about 350 W).

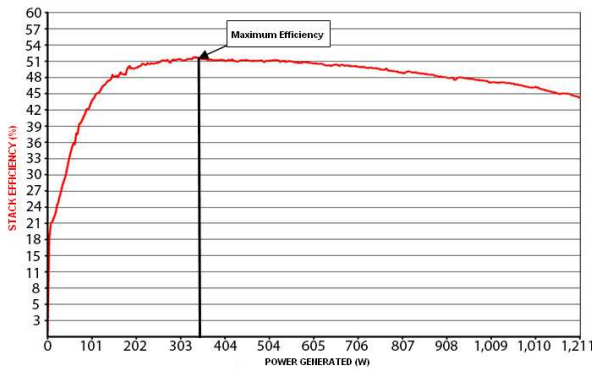


Fig. 7. Efficiency curve of the fuel cells.

Figure 8 shows the efficiency of the stack with an increasing demanded power ramp up to 1,200 W and a decreasing ramp to zero after five minutes. Efficiency is greater in the power generated ramp down, because the stack temperature has risen during the test, demonstrating that stack efficiency is optimal when operates about 65°C.

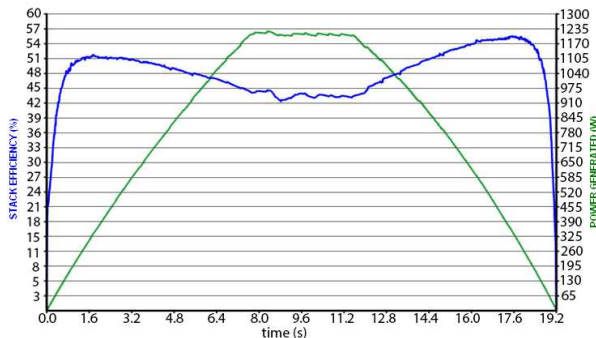


Fig. 8. Stack efficiency and power generated by the fuel cell.

Given these conditions, a control strategy that seeks to maximize the energy efficiency of the micro-grid has been defined.

Thus, three possible power demand cases have been discriminated, 0 to 350W, 350W to 1,550W and 1,550W to 2,400W. In each of these three cases, one of the Boost converters works controlling the voltage and the other works controlling the current which the fuel cell delivers. This is achieved by imposing the duty cycle to each converter, according to the circumstances under which the system is working (power demand, operating temperature, etc.), maximizing the efficiency of the system.

In this way, the control of the power delivered by each fuel cell is achieved. If certain power is demanded from the fuel cells, and one of them has the delivery current limited, the other fuel cell is forced to hand over the rest of current to meet the required load demand.

When selecting which is the Boost to be connected to the fuel cell that is in charge of making the voltage control, the stack temperatures come into play. The approach chosen is that the fuel cell that has the stack at higher temperature will be responsible for carrying out the voltage control. Following, the reason for these selected

criteria is explained, in terms of power and temperature, analysing the different sections of power demanded by the load:

1) Section 1: 0 to 350 W

The fuel cell efficiency is increased up to 350W, so the best option is to deliver power only by a single fuel cell. In this case, the fuel cell that has the hottest stack will start in voltage mode.

2) Section 2: 350 W to 1,550 W

Once achieved 350W by the fuel cell working in voltage mode, the other fuel cell that is in standby mode comes into operation. This way, it is achieved that one of the fuel cells is operating with optimum efficiency.

Considering the fuel cell that operates in current mode, giving more power, it is going to heat more, and the higher the stack temperature is, the greater its efficiency [12]. Thus, one stack achieves efficiency optimization in terms of power delivered, and the other stack increases efficiency due to the heating of the stack.

3) Section 3: 1,550 W to 2,400 W

In this section, the fuel cell which is being regulated to deliver the current reaches its rated power. At this point, the stack that was delivering 350 W starts to deliver the remaining power demanded.

C. Control Algorithm

To control the duty cycle of the MOSFETs working on each converter, two PID loops have been implemented in LabVIEW with feedback loops in voltage and current. Table 1 shows the numerical values considered.

The control algorithm is responsible for detecting the temperature difference of the stacks, managing the control mode switching between voltage and current mode and detecting the operation case depending on the sections.

Table 1. Control parameters

Parameter	PI voltage	PI current
High limit	30	30
Low limit	0	0
Proportional gain (Kc)	0.012	0.005
Integral time (Ti, min)	3.33e-5	3.33e-5
Derivative time (Td, min)	0	0

There are certain situations where it is necessary to stop the system by cutting off the MOSFETs. A clear case, for example, appears when a short circuit occurs and any battery current exceeds 50 A. This situation produces an error in the fuel cells control system and affects their useful life.

To avoid these situations, the developed algorithm incorporates a software protection that is complementary to the physical protection of the fuse.

#### 4. Microgrid's behaviour

Several tests have been developed to verify the correct operation of the microgrid shown in figure 9. On this microgrid, the developed control algorithm has been implemented.



Fig. 9. Microgrid system.

Figure 10 shows the microgrid's control panel implemented in LabVIEW, with screens for output voltage and current during startup of each PEMFC stacks. In this case, system control is disabled. The DC bus voltage is 26.3 volts corresponding to the Nexa Power Module, which is already in operation. Then, there is a power surge which is stabilized at 27.5 V, corresponding to the start of the Nexa Training System. Current is zero for the two PEMFCs. The signal that appears corresponds to the noise produced by the circuit wiring and the transducer.

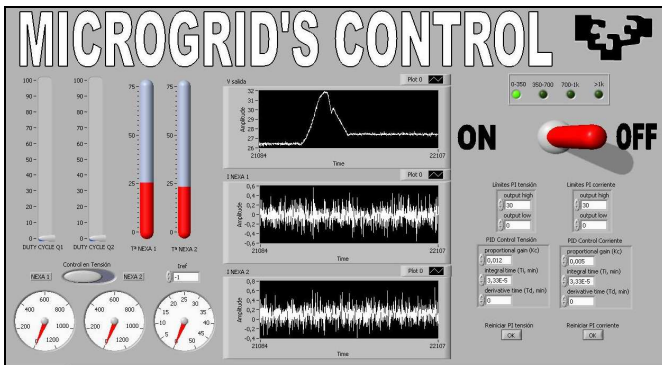


Fig. 10. Microgrid's control panel during system start.

Figure 11 shows the voltage ripple in detail, once started with no-load. This ripple is 0.1 V.

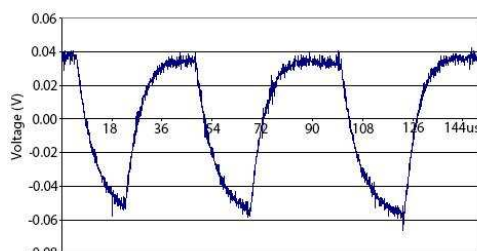


Fig. 11. Converter output voltage ripple.

In the test presented in Figure 12, an increasing power ramp up to 1,900 W has been demanded and, subsequently, a decreasing ramp to zero. In that figure, the three power sections mentioned in 3.2 can be clearly seen. The power of the current controlled fuel cell (Nexa 2) is set to 900 W maximum, while the voltage controlled fuel cell (Nexa 1) can reach its maximum power output.

During section 1, Nexa 2 remains on standby and Nexa 1 delivers power to the load while controlling the output voltage. Once in section 2, Nexa 2 begins to supply increasing power while power of Nexa 1 remains at 350 W. Finally, in section 3, Nexa 2 gives a fixed power about 900 W, while the rest of power is supplied by Nexa 1.

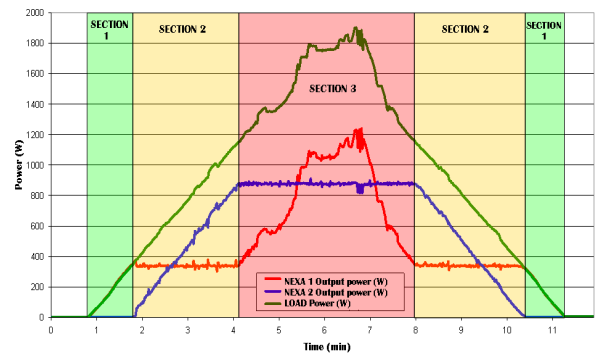


Fig. 12. Power generated by the fuel cells and power consumed by the electronic loads.

Observing Figure 12, it can be seen that the change from section 2 to section 3 takes place when the load consumes 1,200 W. But the total power generated by the two fuel cells in changing those sections is 1,550 W, as shown in Figure 13 (time = 4 min).

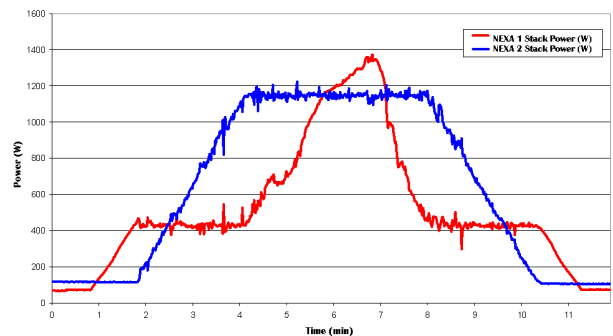


Fig. 13. Power generated by the fuel cell stacks.

Therefore, the power shown in Figure 12 is delivered to the load, while the rest of each stack power generated by each fuel cell is intended to supply auxiliary loads (fans, compressors, control boards) and its own microgrid control system.

Additionally, results of a test developed to verify the optimization achieved are also shown. In this test, a current ramp up to 45 A (1,350 W) is demanded. Then, the system is maintained in such power demand for 2 minutes. Finally, the power demand is increased up to 66 A (2 kW). Figures 14 and 15 show the output power and efficiency of each fuel cell during the test. It can be seen that there is a part of Nexa 1 efficiency which is

maintained constant at its maximum value, due to the implemented control system, improving the system efficiency and reducing the consumption of hydrogen (\*). Subsequently, the efficiency drops because the fuel cell begins to deliver more power as it is demanded. In the case of Nexa 2 efficiency, there is a section in which an increase of this efficiency can be distinguished due to the increased temperature of the stack (\*\*).

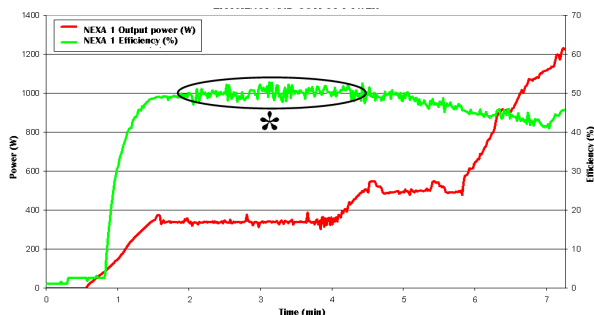


Fig. 14. Efficiency and output power of NEXA 1, during the test.

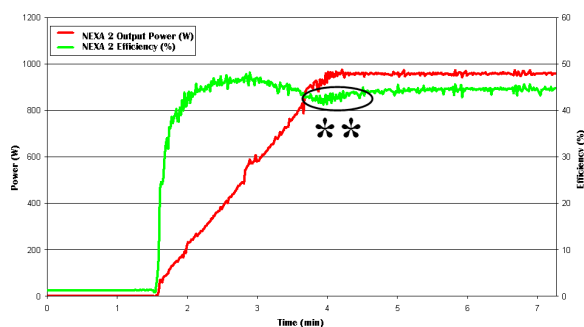


Fig. 15. Efficiency and output power of NEXA 2, during the test.

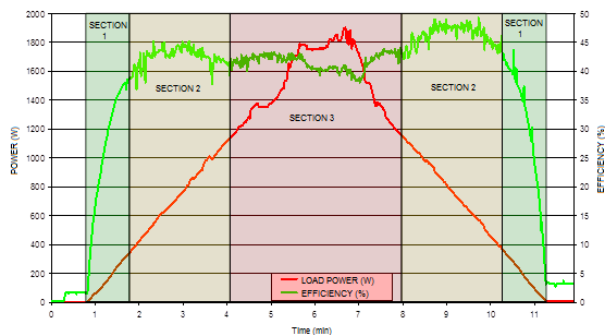


Fig. 16. Global efficiency and output power during the test.

Nexa 2 has delivered more power than Nexa 1 and therefore has heated more than Nexa 1. The system detects this temperature difference, so Nexa 2 continues on current control mode, which causes an increased efficiency, in the down ramp, of 4% compared with the efficiency obtained in the ramp up, as shown in Figure 16.

The overall efficiency is reached in the second section, with an approximate value of 48%.

## 5. Conclusions

This paper has presented the design and implementation of an algorithm to optimize the efficiency of several fuel

cells, when operating together in a microgrid. Some results of experimental tests that allow the evaluation of the power and current demanded by the load and the efficiency achieved have been presented.

The system responds well to load changes and set-point changes, but the response is a bit slow. This slowness is caused by low proportional gain of PI. However, if this gain is increased, oscillations that occur before set-point or load changes are greater. In this case, reducing oscillations and ripple has prevailed instead of speed of response. The performance obtained in terms of output voltage ripple (0.1 V) approximates to that which has been taken into account when designing the converters to control the microgrid (3% of the output voltage).

Also, it has been validated that the implemented algorithm control has improved the efficiency of the system. Through this management an efficiency raising of 4% or remaining it constant for longer has been achieved.

## Acknowledgement

The work presented in this chapter has been supported by the Basque Government (Ref. IT532-10) and by the University of the Basque Country UPV/EHU (Ref. UFI 11/28)

## References

- [1] L. Chiari, A. Zecca, "Constraints of fossil fuels depletion on global warming projections", *Energy Policie*, Vol. 39 pp. 5026–5034 2011.
- [2] I. Roos, S. Soosaar, A. Volkova, D. Streimikene, "Greenhouse gas emission reduction perspectives in the Baltic States in frames of EU energy and climate policy", *Renewable and Sustainable Energy Reviews*, Vol. 16 pp. 2133–2146, 2012.
- [3] NEXA\_ power module user's manual. Ballard Power Systems Inc.; 2003.
- [4] Nexa Training System, 1.2 kW Fuel Cell Training System for System Dimensioning and Hybridization. 2011
- [5] P. Bilski, W. Winiecki, "Methods of assessing the time efficiency in the virtual measurement systems", *Computer Standards & Interfaces* Vol. 34 pp. 485–492, 2012
- [6] K. Baltaci, F. Yildiz, "NI LabView Data Acquisition System Design using Hydrogen Fuel Cell", *Application of Information and Communication Technologies. International Conference on*, pp. 1-6, 2009. Baku (Azerbaijan).
- [7] <http://www.coilws.com/images/E70340-015%20Rev%20A1-Web.pdf>
- [8] <http://datasheet.octopart.com/SMG50VB471M10X20LL-United-Chemi-Con-datasheet-833.pdf>
- [9] <http://www.datasheetcatalog.org/datasheet/stmicroelectronics/3449.pdf>
- [10] <http://www.irf.com/product-info/datasheets/data/aurf1010z.pdf>
- [11] <http://www.intersil.com/content/dam/Intersil/documents/fn71/fn7113.pdf>
- [12] J.I. San Martín, I. Zamora, J.J. San Martín, V. Aperribay, P. Eguía, "Trigeneration Systems with Fuel Cells" *ICREPQ'08*, March-2008. Santander (Spain).